JACS
JOURNAL OF THE AMERICAN CHEMICAL SOCIETY
Communication
pubs.acs.org/JACS

Kr/Xe Separation over a Chabazite Zeolite Membrane

Xuhui Feng,[†] Zhaowang Zong,[†] Sameh K. Elsaidi,[‡] Jacek B. Jasinski,[§] Rajamani Krishna,[∥] Praveen K. Thallapally,*[,‡] and Moises A. Carreon*[,†]

[†]Chemical and Biological Engineering Department, Colorado School of Mines, Golden, Colorado 80401, United States
[‡]Pacific Northwest National Laboratory, Richland, Washington 99352, United States
[§]Conn Center for Renewable Energy Research, University of Louisville, Louisville, Kentucky 40292, United States
[∥]Van 't Hoff Institute for Molecular Sciences, University of Amsterdam, Science Park 904, 1098 XH Amsterdam, The Netherlands

Supporting Information

ABSTRACT: Herein we demonstrate that chabazite zeolite SAPO-34 membranes effectively separated Kr/Xe gas mixtures at industrially relevant compositions. Control over membrane thickness and average crystal size led to industrial range permeances and high separation selectivities. Specifically, SAPO-34 membranes can separate Kr/Xe mixtures with Kr permeances as high as 1.2×10^{-7} mol/m^2 s Pa and separation selectivities of 35 for molar compositions close to typical concentrations of these two gases in air. In addition, SAPO-34 membranes separated Kr/Xe mixtures with Kr permeances as high as 1.2×10^{-7} mol/m^2 s Pa and separation selectivities up to 45 for molar compositions as might be encountered in nuclear reprocessing technologies. Molecular sieving and differences in diffusivities were identified as the dominant separation mechanisms.

The separation of krypton from xenon is an industrially relevant problem. Kr and Xe are widely used in fluorescent light bulbs. High-purity Xe has been used in commercial lighting, medical imaging, anesthesia, and neuroprotection.[1] The current conventional technology produces these gases from the cryogenic distillation of air in which these noble gases are present in very small concentrations (1.14 ppmv Kr, 0.086 ppmv Xe).[2] Typically, both Kr and Xe separate into the oxygen-rich stream after distillation and are concentrated and purified to produce an 80/20 molar mixture of Kr to Xe.[3] This final mixture undergoes cryogenic distillation to produce pure Kr and pure Xe. However, cryogenic distillation is an energy-intensive and expensive process. In addition, separating Kr from Xe is an important issue for nuclear industries. Specifically, separating Kr from Xe is a critical step in removing radioactive ^{85}Kr during treatment of spent nuclear fuel.[3] Effectively separating Kr from Xe in nuclear reprocessing plants would lead to a considerable reduction in storage costs and in potential revenue generated from the sale of pure Xe. The conventional method to separate these two gases is fractional distillation at cryogenic temperatures, which is again an energy intensive process. Furthermore, even after cryogenic distillation, trace levels of radioactive Kr are too high to permit further use. Membrane technology could play a key role in making this separation less energy intensive and economically feasible. Membrane separation process is a viable energy-saving method since it does not involve any phase transformation; furthermore, the required membrane process equipment is simple and easy to operate, control, and scale-up.

Based on the kinetic diameter of Kr (3.69 Å) and Xe (4.10 Å), in principle, SAPO-34, a chabazite small pore zeolite silicoaluminophosphate displaying average pore size of 3.8 Å and having the composition $Si_xAl_yP_zO_2$ where $x = 0.01-0.98$, $y = 0.01-0.60$, and $z = 0.01-0.52$[4] represents an ideal candidate in membrane form to molecular sieve Kr from Xe. The first example of a continuous SAPO-34 membrane was reported almost two decades ago.[5] Since 1998, Noble and Falconer groups have pioneered and demonstrated the successful synthesis of high-performance SAPO-34 membranes able to efficiently separate diverse gas mixtures involving mainly CO_2, H_2, CH_4, and other light hydrocarbons.[6−15] The sharp molecular sieving properties of SAPO-34 membranes have been demonstrated for diverse industrial relevant molecular gas separations, including mainly CO_2/CH_4,[6−16] CO_2/N_2,[16,17] CO_2/butane,[15] and N_2/CH_4.[15,18−20] In all these cases, the smaller molecules diffuse rapidly through the pores of SAPO-34, while the larger molecules at most diffuse slowly, translating into high separation selectivities. Herein, we demonstrate the ability of SAPO-34 membranes to effectively separate Kr/Xe gas mixtures at industrially relevant compositions. SAPO-34 membranes were synthesized by secondary seeded growth on porous tubular α-Al_2O_3 supports at different molar ratios of water to allow membrane thickness control. Membrane synthesis procedure is given in the Supporting Information. The XRD patterns (Figure S1) of the SAPO-34 crystals collected from membrane synthesis were essentially identical for all water mole contents, and the peak position and intensity match those of the simulated chabazite topology typical of SAPO-34.[21] Figure 1 shows representative SEM images of SAPO-34 membranes synthesized with different water contents. Top view SEM images (Figure 1a−e) show well-intergrown and interconnected micron range zeolite crystals. Cross-sectional SEM images of the membranes (Figure 1a′−e′) show dense membrane layers with thickness ranging from ∼3.0 to ∼8.7 μm. The thickness of the membranes decreased as the water content increased.

SAPO-34 membranes were used to separate premixed 9:1 Kr/Xe (Kr rich composition). This composition is close to typical concentrations of these two gases in air and 9:91 Kr/Xe mixtures

Received: June 23, 2016
Published: July 27, 2016

DOI: 10.1021/jacs.6b06515
J. Am. Chem. Soc. 2016, 138, 9791−9794

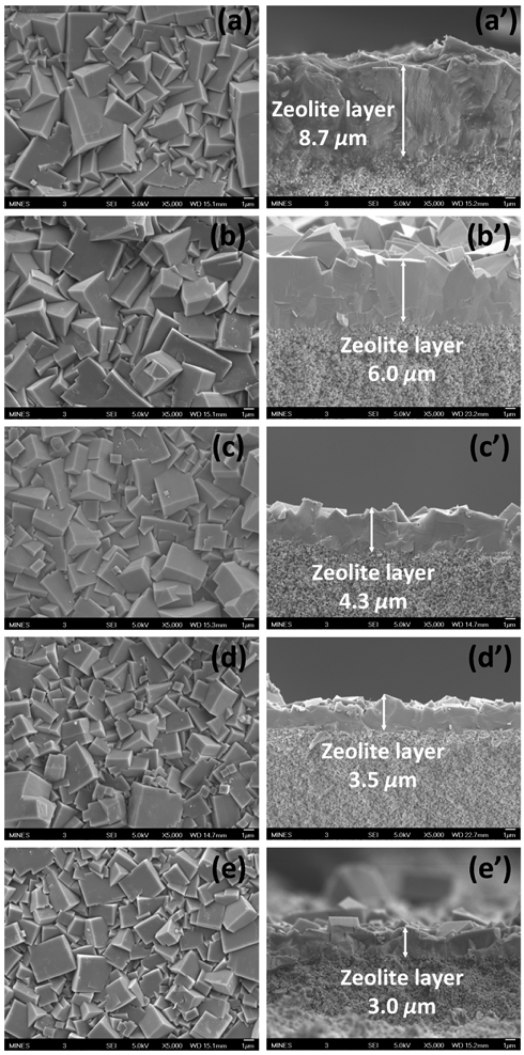

Figure 1. Top view (left) and cross-sectional SEM (right) images of SAPO-34 membranes. Gel composition: 1.0 Al_2O_3/1.0 P_2O_5/0.3 SiO_2/1.0 tetraethylammonium hydroxide (TEAOH)/1.6 dipropylamine (DPA)/x H_2O: (a,a′) x = 150, (b,b′) x = 200, (c,c′) x = 250, (d,d′) x = 300, and (e,e′) x = 350.

(Xe rich composition). This composition corresponds to that encountered in nuclear reprocessing technologies). The feed pressure was 223 kPa, and the pressure in the permeate side was 85 kPa. The separation results at room temperature for these membranes are shown in Table 1. For the Kr rich composition,

Table 1. Kr/Xe Separation Performance over SAPO-34 Membrane[a]

		feed molar composition: 9:1 Kr/Xe		feed molar composition: 9:91 Kr/Xe	
water content	membrane thickness (μm)	Kr permeance (mol/m^2 s Pa) × 10^{-7}	selectivity	Kr permeance (mol/m^2 s Pa) × 10^{-7}	selectivity
x = 150	8.7	0.19	13	0.19	14
x = 200	6.0	0.75	20	0.45	15
x = 250	4.3	1.0	35	0.87	45
x = 300	3.5	1.1	26	1.4	28
x = 350	3.0	1.2	31	1.8	44

[a]Transmembrane pressure = 138 kPa.

Kr permeances correlated well with membrane thicknesses (Figure S2). The thinner the membrane, the higher the Kr permeance. Kr permeances ranged from 0.19 to 1.2 × 10^{-7} mol/m^2 s Pa. Kr/Xe separation selectivities ranged from 13 to 35. In general, separation selectivities improved for the more diluted gel compositions. The best separation selectivities were observed for membranes with water molar contents of 250 and 350 (Figure S2). For the Xe rich composition, Kr permeances correlated well with membrane thicknesses too. Kr permeances increased as the thickness of the membrane decreased. Kr permeances ranged from 0.19 to 1.8 × 10^{-7} mol/m^2 s Pa. As compared to the Kr rich composition, for the Xe rich composition, Kr/Xe separation selectivities were slightly higher, ranging from 14 to 45. The highest separation selectivities were observed for membranes with water molar contents of 250 and 350 (Figure S2). A distinctive feature of the most Kr selective membranes for both gas mixture compositions, (water compositions 250, 300, and 350) is its smaller and narrower crystal size distribution as compared to the less selective membranes (water compositions 150 and 200). In principle, smaller crystal sizes close-pack better[11] leading to higher separation selectivities. The volcano-type behavior observed for the Kr/Xe separation selectivity (Figure S2) may indicate a coupled effect of crystal size and membrane on the Kr/Xe separation performance.

As shown in Figure S3, the two key parameters having a profound effect on Kr permeance and separation selectivities were membrane thickness and membrane average crystal size, respectively. Higher water content (x = 400) resulted in defective membranes that could not hold pressure for a transmembrane drop permeation measurement. In this case, intercrystalline boundaries around SAPO-34 crystals might have resulted in high concentration of defects. The observed high Kr permeances and moderate to high separation selectivities make these SAPO-34 membranes appealing for separating Kr from Xe at industrial relevant compositions. For any potential industrial applications, membrane reproducibility is a key prerequisite. As a representative example, Table S1 shows the separation performance for a premixed 9:1 Kr/Xe mixture of three membranes (x = 300) prepared independently. These membranes displayed similar separation indexes π in the 0.23−0.27 mol/m^2 s range, indicating good reproducibility. Separation index π [π = Kr permeance × (selectivity − 1) × permeate pressure] has been used as a reliable quantitative parameter to predict zeolite membrane reproducibility.[10]

Adsorption isotherms, isosteric heats of adsorption, and column breakthrough experiments were measured for Kr and Xe to help explain the separation mechanisms for the Kr selective membranes. Figure 2a shows the Kr and Xe adsorption isotherms collected at 298 and 278 K for SAPO-34 crystals. The adsorption isotherms at 140 kPa (~transmembrane pressure drop employed for the gas mixture separation experiments) revealed Xe uptakes of 39.9 cm^3/g (1.78 mmol/g) and 46.3 cm^3/g (2.07 mmol/g) at 298 and 278 K, respectively, and Kr uptakes of 14.7 cm^3/g (0.66 mmol/g) and 22.6 cm^3/g (1.01 mmol/g), respectively. Therefore, at 140 kPa and 298 K (prevailing conditions during separation experiments), SAPO-34 adsorbs ~2.7 times more Xe than Kr. Figure 2b shows the isosteric heats of adsorption (Q_{st}) for Kr and Xe calculated by Virial method, using the experimental single adsorption isotherms (Figures S4 and S5). At 1.4 bar, SAPO-34 crystals exhibited Q_{st} values of −24.4 and −17.3 kJ/mol for Xe and Kr, respectively, confirming the preferential adsorption of Xe over Kr on SAPO-34. These Q_{st} values are higher than those reported for activated carbon[22] and HKUST-

DOI: 10.1021/jacs.6b06515
J. Am. Chem. Soc. 2016, 138, 9791−9794

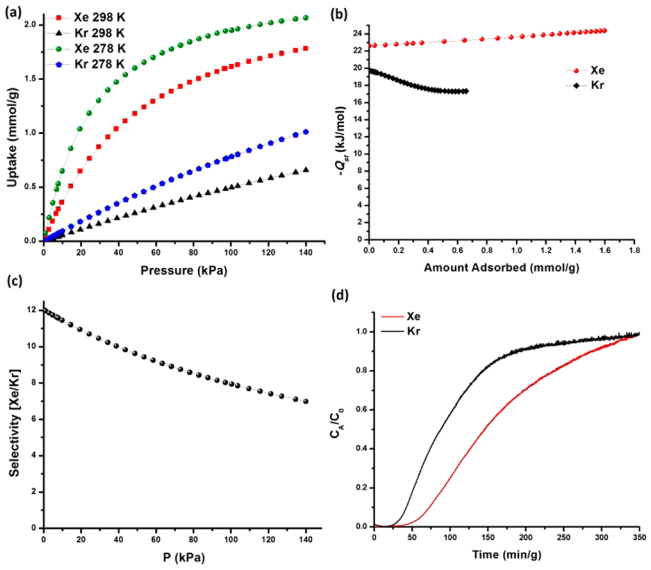

Figure 2. (a) Single component Xe and Kr adsorption isotherms collected at 298 and 278 ., (b) Xe and Kr isosteric heats of adsorption (Q_{st}) calculated by Virial method. (c) IAST calculated selectivity for 91:9 Xe/Kr gas mixture at 298 K. (d) Column breakthrough experiment for 91:9 Xe/Kr gas mixture at 298 K and 140 kPa for SAPO-34 crystals.

1[22−24] and comparable to those of Ni-MOF-74[22,23] and Mg-MOF-74.[23] Ideal adsorbed solution theory (IAST) was used to predict the selectivity of Xe over Kr binary mixture based on the experimental single adsorption isotherms collected at 298 K. The single-component isotherms were fit to a Langmuir−Freundlich eq (Figures S6 and S7). At 140 kPa and 298 K the adsorption selectivity for a 91:9 Xe/Kr binary gas mixture was calculated to be ∼7 (Figure 2c), confirming again that Xe adsorbs stronger than Kr. The preferential adsorption of Xe over Kr in SAPO-34 can be explained by differences in dipole polarizabilities of these two molecules. Xe has higher dipole polarizability (26.85−28.7 atomic units) as compared to Kr (16.44−18.0 atomic units).[25] Due to local electronegativity differences between framework Si, Al, and P, SAPO-34 has anionic framework with a net negative charge depending upon how the silicon substitution into the framework.[26] Therefore, stronger electrostatic interactions between the negatively charged SAPO-34 surface and the higher dipole moment of Xe promotes its preferential adsorption over Kr. The preferential adsorption of larger molecules over smaller molecules has been observed in chabazite zeolite crystals.[27] In addition, the preferential adsorption of Xe over Kr on different porous crystalline materials, including zeolites and metal−organic frameworks (MOFs), is well documented. For example, zeolite NaX has been used as a selective adsorbent for Xe over Kr with a selectivity of ∼6 with Kr concentrations ranging from 1 to 10,000 ppm.[3] Zeolite NaA displayed a selectivity of ∼4 for binary mixtures of Xe and Kr at 300 K between 100 and 1000 kPa.[28] Adsorption Xe selectivity over Kr has been observed in MOFs, too.[1,22,29−32] The leading sorbent material for Xe/Kr separation is the porous organic cage CC3, which was shown to separate 400 ppm Xe from 40 ppm Kr in air with a Xe/Kr selectivity of ∼20.4.[1] In the case of MOFs, the selectivity to Xe arised from the fact that Xe is a more polarizable molecule than Kr, which tends to form stronger van der Waals interactions with the open metal centers of MOFs. In the case of CC3, the selectivity to Xe was attributed to a precise size match between Xe and the organic cage cavity.

In principle, the preferential adsorption of Xe would favor separating Xe over Kr in the gas mixture. However, the smaller Kr molecule should diffuse faster than the larger Xe molecule. Column breakthrough experiments were conducted to learn about the relative diffusivity differences between Kr and Xe over SAPO-34 crystals (Figure 2d). For a 91:9 gas mixture at 298 K, the breakthrough time for Kr was 22 min, and for Xe, 39 min for 1 g of sample at flow rate of 1 mL/min and pressure of 140 kPa, indicating higher diffusivity of Kr over Xe. This was expected since Kr has lower capacity and affinity to SAPO-34 diffusing out from the column faster (breakthrough first), while Xe having higher affinity and capacity to SAPO-34 will breakthrough later. Therefore, differences in diffusivity favor the separation of Kr over Xe in the gas mixture. Differences in diffusivities leading to Kr/Xe ideal separation selectivities of ∼11.8 over SAPO-34 membranes grown on porous alumina disks have been reported.[33] Molecular gas mixtures can be separated over zeolite membranes by at least one of the following separation mechanisms: molecular sieving, differences in diffusivity, and competitive adsorption. Based on the kinetic diameter of Kr (3.69 Å) and Xe (4.10 Å), SAPO-34 membranes can separate these gases by molecular sieving. In addition, to this mechanism, breakthrough experiments (Figure 2d) demonstrate higher diffusivity of Kr over Xe. Since separation selectivities for gas mixtures (Table 1 and Table S2) are moderate, this suggests that Xe can permeate through the pores of SAPO-34. This is not surprising since hydrocarbons such as propane and *n*-butane, having kinetic diameters of ∼4.3 Å (slightly larger size than Xe molecule), can adsorb within the pores of SAPO-34.[34] Adsorption experiments show that Xe adsorbs more strongly than Kr on SAPO-34 crystals, favoring the separation of Xe over Kr in the gas mixture. Although competitive adsorption and diffusivity/molecular sieving compete as separation mechanisms, separation data suggest that diffusivity differences and molecular sieving are the two dominant mechanisms leading to highly permeable Kr selective membranes.

In order to gain further insights into intracrystalline diffusivities of Xe and Kr, we carried out simulations of membrane permeation and transient breakthroughs using the methodologies detailed in the literature.[35−37] The simulation details are included in the Supporting Information (Figure S8−S11). On the basis of the simulations, we can conclude that the membrane permeation experiments can be rationalized if the intracrystalline diffusivity of Kr is about 2 orders of magnitude higher than that of Xe. The transient breakthrough experiments also indicate that diffusivity of Kr is significantly higher than that of Xe.

Few membranes have been proposed to separate Kr and Xe (Table S2). However, all these membranes have been evaluated only for *single gas* permeation experiments and not for *gas mixtures*. Furthermore, these membranes show low *ideal* separation selectivities and low Kr permeances.

A membrane prepared with 350 mol water content was evaluated for the molar gas mixture composition of 9:91 Kr/Xe at transmembrane pressure of 700 kPa, which is the typical pressure at which Kr and Xe may enter to the column cryogenic distillation process.[38] As expected, and mainly due to concentration polarization, both Kr permeance and Kr/Xe separation selectivity decreased to 0.19×10^{-7} mol/m^2 s Pa and 13, respectively. Despite this decrease, SAPO-34 membranes still display moderate Kr permeances and Kr/Xe separation selectivities at such high pressure.

DOI: 10.1021/jacs.6b06515
J. Am. Chem. Soc. 2016, 138, 9791−9794

In summary, we have demonstrated the ability of SAPO-34 membranes to effectively separate Kr/Xe gas mixtures at industrially relevant compositions. Membrane thickness and average crystal size were key parameters that profoundly affected membrane separation performance. Thinner membranes with smaller and narrower crystal size led to industrial range permeances and high separation selectivities. SAPO-34 membranes separated Kr/Xe mixtures with Kr permeances as high as 1.2×10^{-7} mol/m^2 s Pa and separation selectivities of 35 for molar compositions close to typical concentrations of these two gases in air. In addition, SAPO-34 membranes separated Kr/Xe mixtures with Kr permeances as high as 1.2×10^{-7} mol/m^2 s Pa and separation selectivities up to 45 for molar compositions as might be encountered in nuclear reprocessing technologies. Diffusivity differences and molecular sieving were the two dominant separation mechanisms. The high Kr permeances and high separation selectivities make these membranes appealing for separating Kr/Xe mixtures at industrial relevant compositions, and potentially as a more economic and less energy intensive alternative to cryogenic distillation, the benchmark technology used to separate these gas mixtures.

■ ASSOCIATED CONTENT

Supporting Information

The Supporting Information is available free of charge on the ACS Publications website at DOI: 10.1021/jacs.6b06515.

Experimental methods and gas sorption studies/calculations (PDF)

■ AUTHOR INFORMATION

Corresponding Authors

*praveen.thallapally@pnnl.gov

*mcarreon@mines.edu

Notes

The authors declare no competing financial interest.

■ ACKNOWLEDGMENTS

We gratefully acknowledge the financial support by the Department of Energy (DOE) Nuclear Energy University Program (NEUP) under Grant No. DE-NE0008429.

■ REFERENCES

(1) Chen, L.; Reiss, P. S.; Chong, S. Y.; Holden, D.; Jelfs, K. E.; Hasell, T.; Little, M. A.; Kewley, A.; Briggs, M. E.; Stephenson, A.; Thomas, K. M.; Armstrong, J. A.; Bell, J.; Busto, J.; Noel, R.; Liu, J.; Strachan, D. M.; Thallapally, P. K.; Cooper, A. I. *Nat. Mater.* **2014**, *13*, 954−960.

(2) Kerry, F. G. *Industrial Gas Handbook: Gas Separation and Purification*; CRC Press/Taylor & Francis Group: Boca Raton, FL, 2007.

(3) Izumi, J. Waste gas treatment using zeolites in nuclear-related industries. In *Handbook of Zeolite Science and Technology*; Auerbach, S. M., Carrado, K. A., Dutta, P. K., Eds.; Marcel Dekker, New York, 2003.

(4) Szostak, R. *Molecular Sieves-Principles of Synthesis and Identification*; Van Nostrand Reinhold: New York, 1989.

(5) Lixiong, Z.; Mengdong, J.; Enze, M. *Stud. Surf. Sci. Catal.* **1997**, *105*, 2211−2216.

(6) Poshusta, J. C.; Tuan, V. A.; Falconer, J. L.; Noble, R. D. *Ind. Eng. Chem. Res.* **1988**, *37*, 3924−3929.

(7) Poshusta, J. C.; Tuan, V. A.; Pape, E. A.; Noble, R. D.; Falconer, J. L. *AIChE J.* **2000**, *46*, 779−789.

(8) Ping, E. W.; Zhou, R.; Funke, H. H.; Falconer, J. L.; Noble, R. D. *J. Membr. Sci.* **2012**, *415−416*, 770−775.

(9) Zhou, R.; Ping, E. W.; Funke, H. H.; Falconer, J. L.; Noble, R. D. *J. Membr. Sci.* **2013**, *444*, 384−393.

(10) Carreon, M. A.; Li, S.; Falconer, J. L.; Noble, R. D. *Adv. Mater.* **2008**, *20*, 729−732.

(11) Carreon, M. A.; Li, S.; Falconer, J. L.; Noble, R. D. *J. Am. Chem. Soc.* **2008**, *130*, 5412−5413.

(12) Li, S.; Falconer, J. L.; Noble, R. D. *Adv. Mater.* **2006**, *18*, 2601−2603.

(13) Li, S.; Falconer, J. L.; Noble, R. D. *J. Membr. Sci.* **2004**, *241*, 121−135.

(14) Funke, H. H.; Chen, M. Z.; Prakash, A. N.; Falconer, J. L.; Noble, R. D. *J. Membr. Sci.* **2014**, *456*, 185−191.

(15) Wu, T.; Diaz, M. C.; Zheng, Y.; Zhou, R.; Funke, H. H.; Falconer, J. L.; Noble, R. D. *J. Membr. Sci.* **2015**, *473*, 201−209.

(16) Venna, S. R.; Carreon, M. A. *Langmuir* **2011**, *27*, 2888−2894.

(17) Li, S.; Fan, C. Q. *Ind. Eng. Chem. Res.* **2010**, *49*, 4399−4404.

(18) Huang, Y.; Wang, L.; Song, Z.; Li, S.; Yu, M. *Angew. Chem.* **2015**, *127*, 10993−10997.

(19) Li, S.; Zong, Z.; Zhou, S. J.; Huang, Y.; Song, Z.; Feng, X.; Zhou, R.; Meyer, H. S.; Yu, M.; Carreon, M. A. *J. Membr. Sci.* **2015**, *487*, 141−151.

(20) Zong, Z.; Feng, X.; Huang, Y.; Song, Z.; Zhou, R.; Zhou, S. J.; Carreon, M. A.; Yu, M.; Li, S. *Microporous Mesoporous Mater.* **2016**, *224*, 36−42.

(21) Szostak, R. *Handbook of Molecular Sieves*; Van Nostrand Reinhold: New York, 1992; p 416.

(22) Liu, J.; Thallapally, P. K.; Strachan, D. *Langmuir* **2012**, *28*, 11584−11589.

(23) Perry, J. J., IV; Teich-McGoldrick, S. L.; Meek, S. T.; Greathouse, J. A.; Haranczyk, M.; Allendorf, M. D. *J. Phys. Chem. C* **2014**, *118*, 11685−11698.

(24) Soleimani Dorcheh, A.; Denysenko, D.; Volkmer, D.; Donner, W.; Hirscher, M. *Microporous Mesoporous Mater.* **2012**, *162*, 64−68.

(25) Maroulis, G.; Thakkar, A. J. *J. Chem. Phys.* **1988**, *89*, 7320−7323.

(26) Lok, B. M.; Messina, C. A.; Patton, R. L.; Gajek, R. T.; Cannan, T. R.; Flanigen, E. M. *J. Am. Chem. Soc.* **1984**, *106*, 6092−6093.

(27) Shang, J.; Li, G.; Singh, R.; Gu, Q.; Nairn, K. M.; Bastow, T. J.; Medhekar, N.; Doherty, C. M.; Hill, A. J.; Liu, J. Z.; Webley, P. A. *J. Am. Chem. Soc.* **2012**, *134*, 19246−19253.

(28) Jameson, C. J.; Jameson, A. K.; Lim, H.-M. *J. Chem. Phys.* **1997**, *107*, 4364−4372.

(29) Bae, Y.-S.; Hauser, B. G.; Colón, Y. J.; Hupp, J. T.; Farha, O. K.; Snurr, R. Q. *Microporous Mesoporous Mater.* **2013**, *169*, 176−179.

(30) Wang, H.; Yao, K.; Zhang, Z.; Jagiello, J.; Gong, Q.; Han, Y.; Li. *J. Chem. Sci.* **2014**, *5*, 620−624.

(31) Liu, J.; Strachan, D. M.; Thallapally, P. K. *Chem. Commun.* **2014**, *50*, 466−468.

(32) Ryan, P. J.; Farha, O. K.; Broadbelt, L. J.; Snurr, R. Q.; Bae, Y.-S. Metal−organic frameworks for Xe/Kr separation. U.S. Patent 13,947,406, 2014.

(33) Crawford, P. G. Zeolite membranes for the separation of krypton and xenon from spent nuclear fuel reprocessing off-gas. MS Thesis, Georgia Institute of Technology, Atlanta, GA, 2013.

(34) Agarwal, K.; John, M.; Pai, S.; Newalkar, B. L.; Bhargava, R.; Choudary, N. V. *Microporous Mesoporous Mater.* **2010**, *132*, 311−318.

(35) Krishna, R. *Microporous Mesoporous Mater.* **2014**, *185*, 30−50.

(36) Krishna, R. *Phys. Chem. Chem. Phys.* **2016**, *18*, 15482−15495.

(37) Krishna, R. *RSC Adv.* **2015**, *5*, 52269−52295.

(38) Cabe, J. E.; Bearden, M. D.; Brown, D. R.; Thallapally, P. K.; Strachan, D. M. A preliminary economic study on the use of Metal-Organic-Framework (MOF) materials for Kr capture. Pacific Northwest National Laboratory, US Department of Energy report FCRD-SWF-2014-000035, June 2014.

DOI: 10.1021/jacs.6b06515
J. Am. Chem. Soc. 2016, 138, 9791−9794

Supporting Information

Kr/Xe Separation over a Chabazite Zeolite Membrane

Xuhui Feng,[1] Zhaowang Zong,[1] Sameh Elsaidi,[2] Jacek B. Jasinski,[3] Rajamani Krishna,[4] Praveen K. Thallapally,[2*] Moises A. Carreon[1*]

[1] Chemical and Biological Engineering Department, Colorado School of Mines, Golden, CO 80401, United States

[2] Pacific Northwest National Laboratory, Richland, WA 99352 United States

[3] Conn Center for Renewable Energy Research, University of Louisville, Louisville, KY, 40292 United States

[4]Van 't Hoff Institute for Molecular Sciences, University of Amsterdam, Science Park 904, 1098 XH Amsterdam, The Netherlands.

[*]Corresponding authors: Praveen.Thallapally@pnnl.gov; mcarreon@mines.edu

Materials and Methods

Preparation of SAPO-34 seeds

Seeds were prepared with a gel composition of 1.0 Al_2O_3: 2.0 P_2O_5: 0.6 SiO_2 : 4.0 TEAOH : 150 H_2O. Al source ($Al(i\text{-}C_3H_7O)_3$, ≥99.99%, Sigma-Aldrich) was mixed with deionized water and stirred at room temperature for 1 h, followed by the addition of phosphoric acid (H_3PO_4, ≥85 wt. %, Sigma-Aldrich) and stirring for another 2 h. Then, Ludox AS-40 colloidal silica (SiO_2, 40 wt. % suspension in water, Sigma-Aldrich) was added, and the resultant solution was stirred for another 3 hours. Tetraethylammonium hydroxide (TEAOH, 35 wt. % in water, Sigma-Aldrich) was added and the mixture was stirred overnight at room temperature. The resultant gel was then placed in an autoclave and heated in a microwave oven (CEM Mars 5 Microwave Reaction System with XP-1500 plus control vessel) at 180 ^oC for 7 h. Crystals were collected by

centrifugating the resultant gel at 3300 rpm for 10 min followed washings with deionized water for three times and dried overnight at 100 ^{o}C.

Preparation of gel for membrane growth

The synthesis gel for membrane preparation has a composition of 1.0 Al_2O_3: 1.0 P_2O_5: 0.3 SiO_2: 1.0 TEAOH : 1.6 DPA : *x* H_2O (*x*=150, 200, 250, 300, and 350). Al(*i*-$C_3H_7O)_3$ was used as Al source, 85 wt. % H_3PO_4 was used as P source where as Ludox AS-40 colloidal silica was used as Si source. To prepare the gel, Al(*i*-$C_3H_7O)_3$ was mixed with deionized water and stirred for 1 h to form a homogeneous mixture, followed by addition of phosphoric acid and stirring for another 2 h. Ludox AS-40 colloidal silica was then added and the mixture was stirred for another 3 hours before TEAOH was added. After another 1 h of stirring, DPA (diproprylamine, 99%, Acros Organics) was added to the solution. The solution was then stirred (aged) at 45-50 ^{o}C for 3 days before being used for membrane preparation.

Preparation of SAPO-34 membranes

SAPO-34 membranes were prepared by slightly modifying our previous reported synthesis approach (Micropor. Mesopor. Mater. 2016, 224, 36-42). Alumina tubular supports (10-mm OD, 7-mm ID, 100-nm pores) were purchased from Inopor GmbH. Upon receiving, the alumina tubes were cut into 10-cm long pieces and both of the ends were glazed (Duncan 1001N). The effective permeation area is ~7.5 cm^2. The glazed supports were calcined at 950 ^{o}C for 15 min with heating and cooling rates of 1 ^{o}C/min and treated twice in boiling water for 30 min and dried at 150 ^{o}C overnight.

The supports were seeded by rubbing SAPO-34 seeds with a cotton swab onto the inner surface. The outer surface of the supports was wrapped with Teflon tape to prevent growth of membrane on the outside surface. Seeded supports were placed in Teflon liners filled with synthesis gel. Hydrothermal treatment was then carried out in a conventional oven at 230 ^{o}C for 6 h. After hydrothermal synthesis, the membranes were washed with flowing tap water for 15 min and then dried at 100 ^{o}C for ~2 h. The membranes were then calcined at 400 ^{o}C for 4 h under vacuum condition with a heating and cooling rate of 0.8 ^{o}C/min.

Characterization

Powder X-ray diffraction (PXRD) analysis was conducted on the crystals collected from the bottom of the support tubes during membrane preparation with a X'Pert PRO MPD X-Ray Diffraction System operated at 45 kV and 40 mA with Cu Kα1 radiation (λ=1.54059 Å). SAPO-34 membranes were broken for SEM analysis on a JEOL JSM-7000F scanning electron microscope operated at the accelerating voltage of 5 kV.

Gas Permeation Measurement

Gas mixture permeations were measured in a flow system. The membrane was mounted in a stainless steel module and sealed at each end with silicone O-rings. The pressure on each side of the membrane was independently controlled. Fluxes were measured using a bubble flow meter. For mixture separation, premixed Kr/Xe=9:91 and Kr/Xe=90:10 mixture molar compositions (Advanced Specialty Gases, 99.999%) were used as feed gas. The total feed flow rate was 70 mL/min. The feed pressure was 223 kPa, and the pressure in the permeate side was 85 kPa for a transmembrane pressure of 138 kPa. The compositions of the feed, retentate and permeate streams were measured, after attaining the steady state, using a gas chromatograph (SRI instruments, 8610C) equipped with a thermal conductivity detector and HAYESEP-D packed column. The oven, injector and detector temperatures in the GC were kept at 40 °C, 120 °C and 150 °C, respectively. All selectivities are permselectivities (ratios of permeances). The permeances were calculated as the fluxes divided by the partial pressure driving forces. Because the module has a cross-flow design, a logarithm of the mean partial pressure drop was used to calculate the driving force.

Specifically, the permeance of the component *i*, P_i, was calculated using:

$$P_i = \frac{J_i}{\Delta p_{\ln,i}} \tag{1}$$

where J_i is the flux through the membrane for component *i*. For the cross-flow configuration, one component preferentially permeates through the membrane, so the partial pressures in the feed and retentate sides are quite different. Therefore, a log-mean pressure drop, $\Delta p_{\ln,i}$, was calculated by:

$$\Delta p_{\ln,i} = \frac{(p_{f,i} - p_{r,i})}{\ln[(p_{f,i} - p_{p,i})/(p_{r,i} - p_{p,i})]} \quad (2)$$

where $p_{f,i}$, $p_{r,i}$, and $p_{p,i}$ are partial pressures for component *i,* in feed, retentate, and permeate sides, respectively. The permeability is defined as the permeance multiplied by membrane thickness. The separation selectivity, $\alpha_{i/j}^{sep}$, is the ratio of the permeances of components *i* and *j* in the mixture.

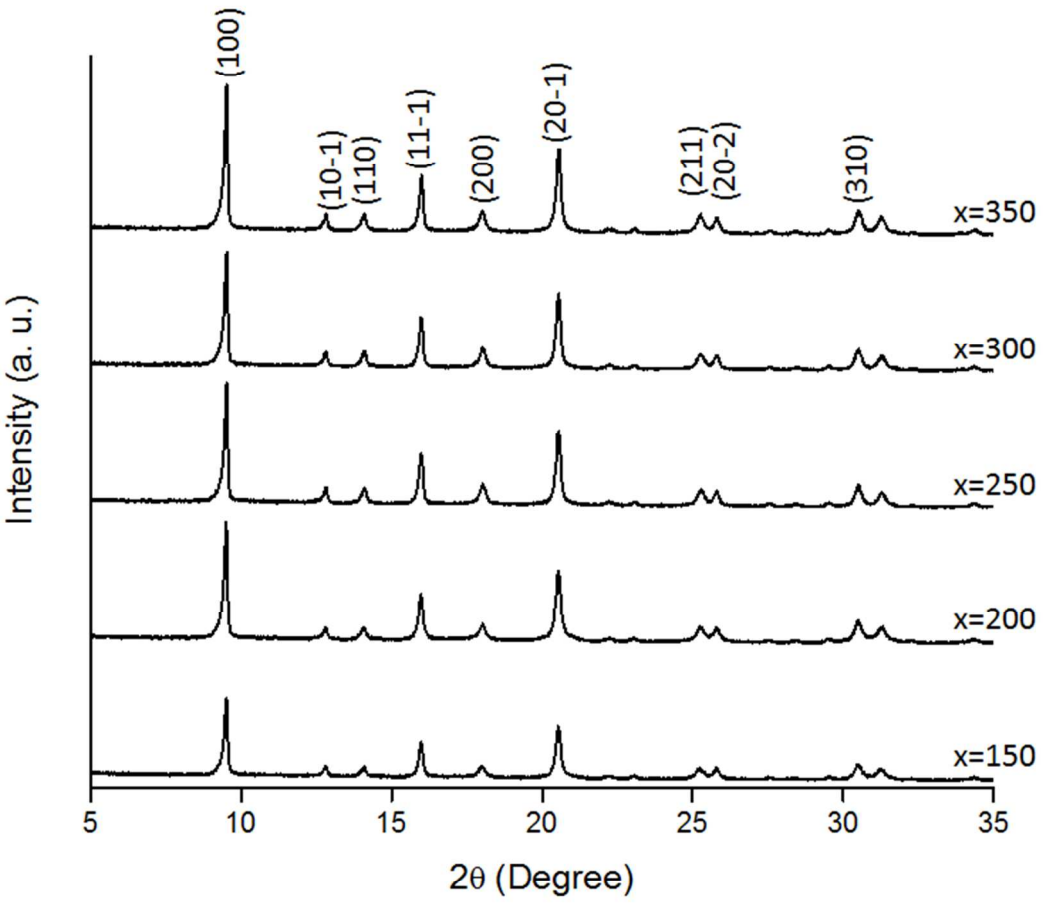

Figure S1. XRD patterns of SAPO-34 powders collected from the bottom of the membrane gel as a function of water molar content.

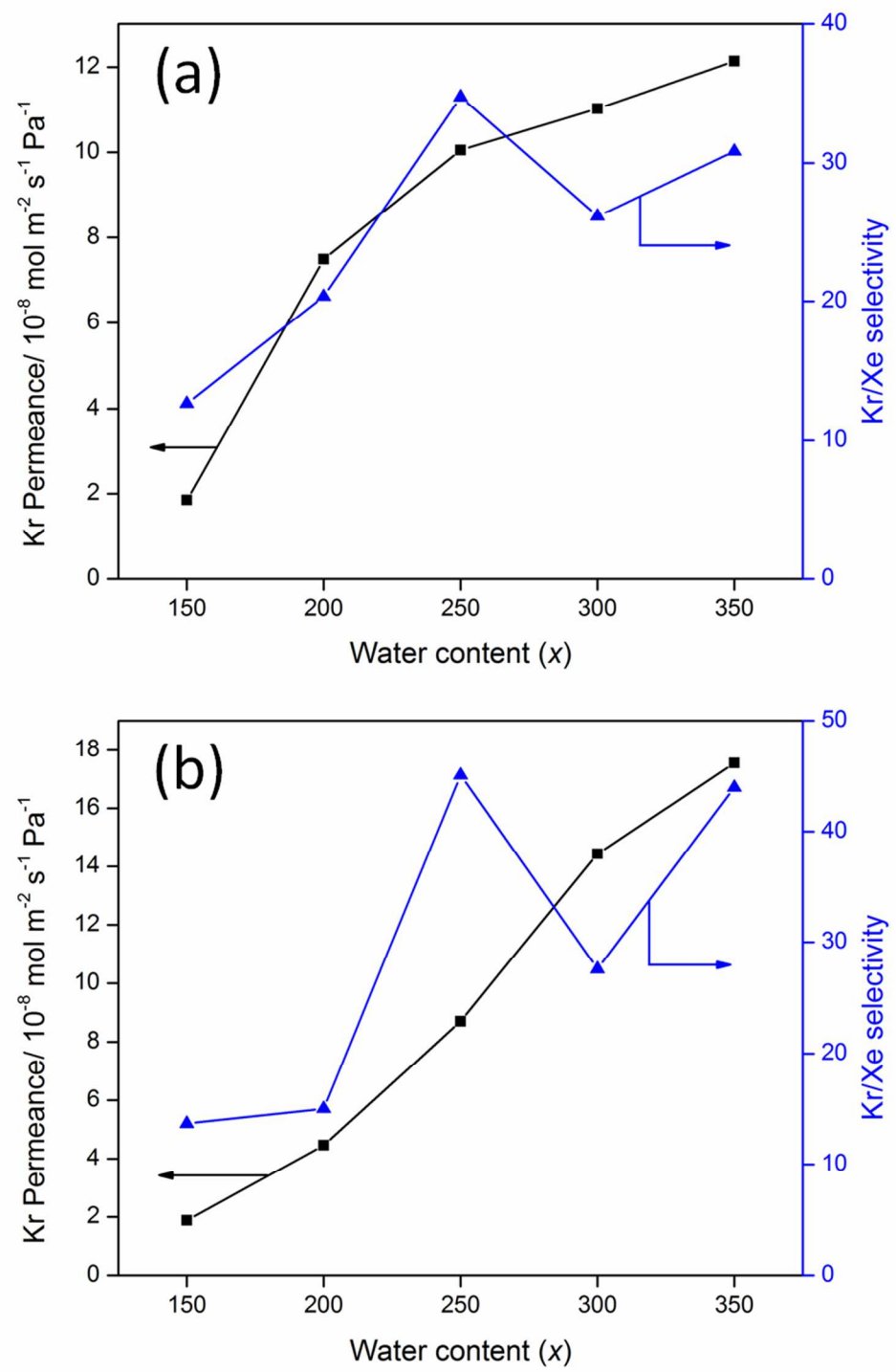

Figure S2. Separation performance of SAPO-34 membranes as a function of water content for molar gas mixture composition of (a) 9:1 Kr/Xe and (b) 9:91 Kr/Xe .

Table S1. Gas mixture separation data illustrating SAPO-34 membrane reproducibility. Molar gas mixture composition: 9:1 Kr/Xe. Feed pressure 223 kPa, and transmembrane pressure 138 kPa. Membranes composition: 1.0 Al_2O_3 : 1.0 P_2O_5 : 0.3 SiO_2 : 1.0 TEAOH : 1.6 DPA : 300 H_2O.

Membrane	Kr Permeance ($mol/m^2 \cdot s \cdot Pa$) $x10^{-7}$	Kr/Xe selectivity	Separation index (π)* ($mol/m^2 \cdot s$)
1	1.1	26	0.23
2	1.2	27	0.27
3	0.97	34	0.27

* π= Kr permeance × (selectivity-1) × permeate pressure

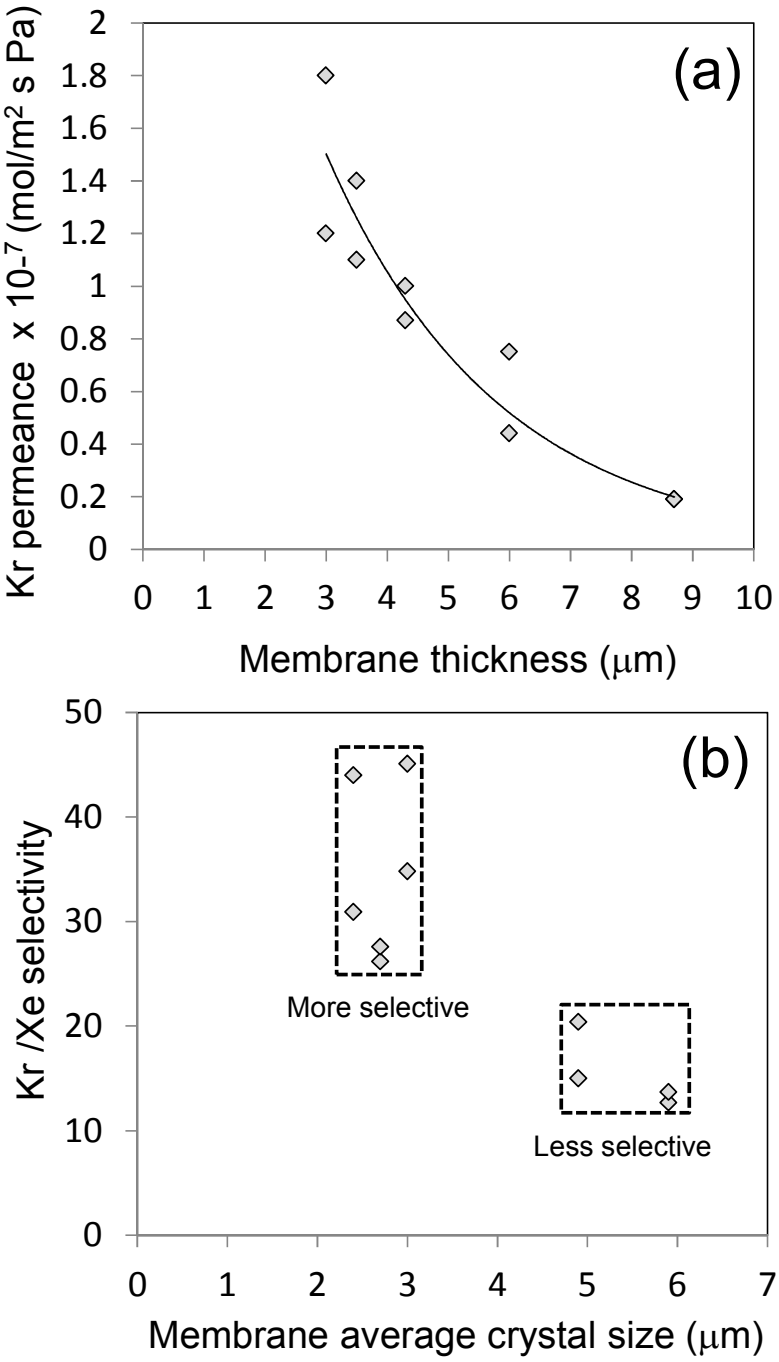

Figure S3. (a) Kr permeance as a function of membrane thickness. (b) Separation selectivity as a function of membrane average crystal size. Membrane average crystal size for the 150, 200, 250, 300, and 350 water mol compositions were 5.9±0.9 μm, 4.8±1.0 μm, 3.0±0.7 μm, 2.7±0.7 μm and 2.4±0.6 μm respectively. Data includes both feed compositions.

Calculation of Isosteric heat of Adsorption (Q_{st}):

The Q_{st} values for Xe and Kr gases were calculated using Virial method as shown in Figures S3 and S4.

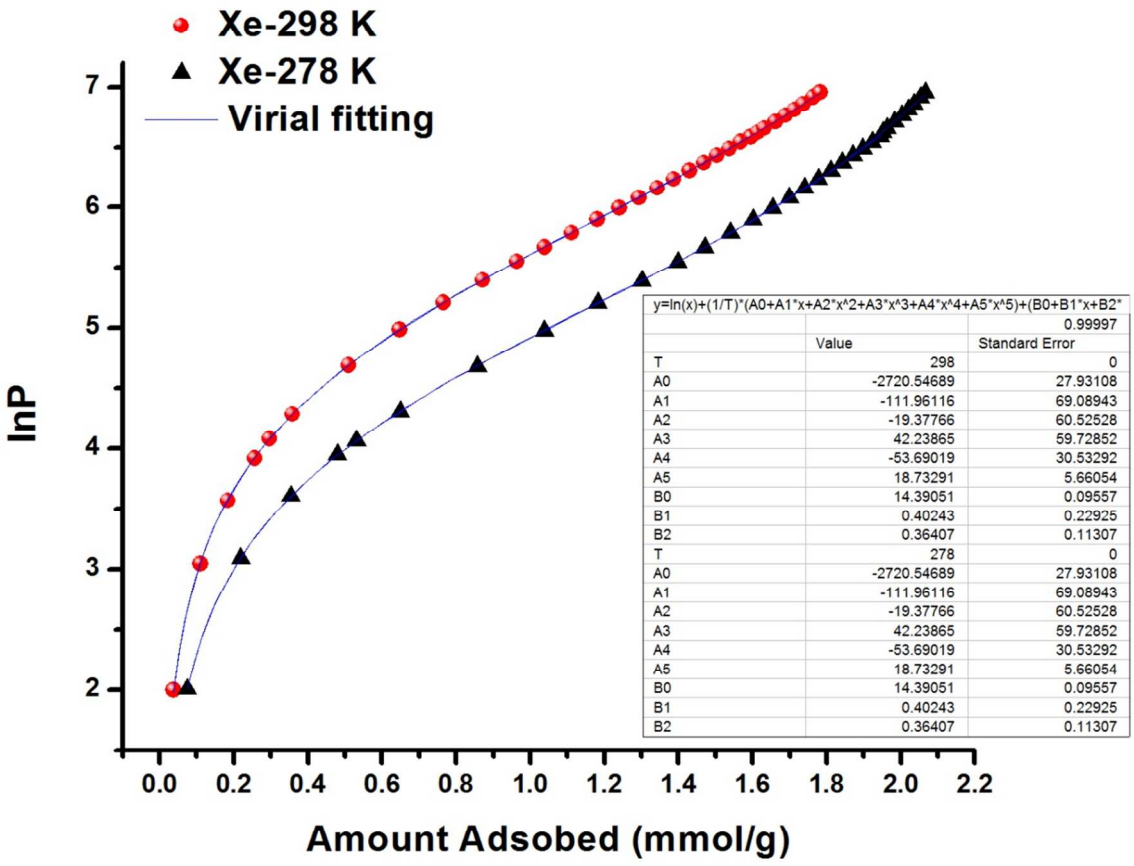

y=ln(x)+(1/T)*(A0+A1*x+A2*x^2+A3*x^3+A4*x^4+A5*x^5)+(B0+B1*x+B2*

		0.99997
	Value	Standard Error
T	298	0
A0	-2720.54689	27.93108
A1	-111.96116	69.08943
A2	-19.37766	60.52528
A3	42.23865	59.72852
A4	-53.69019	30.53292
A5	18.73291	5.66054
B0	14.39051	0.09557
B1	0.40243	0.22925
B2	0.36407	0.11307
T	278	0
A0	-2720.54689	27.93108
A1	-111.96116	69.08943
A2	-19.37766	60.52528
A3	42.23865	59.72852
A4	-53.69019	30.53292
A5	18.73291	5.66054
B0	14.39051	0.09557
B1	0.40243	0.22925
B2	0.36407	0.11307

Figure S4. Xe adsorption isotherm of SAPO-34 at 298 K and 278 K fitted using Virial equation.

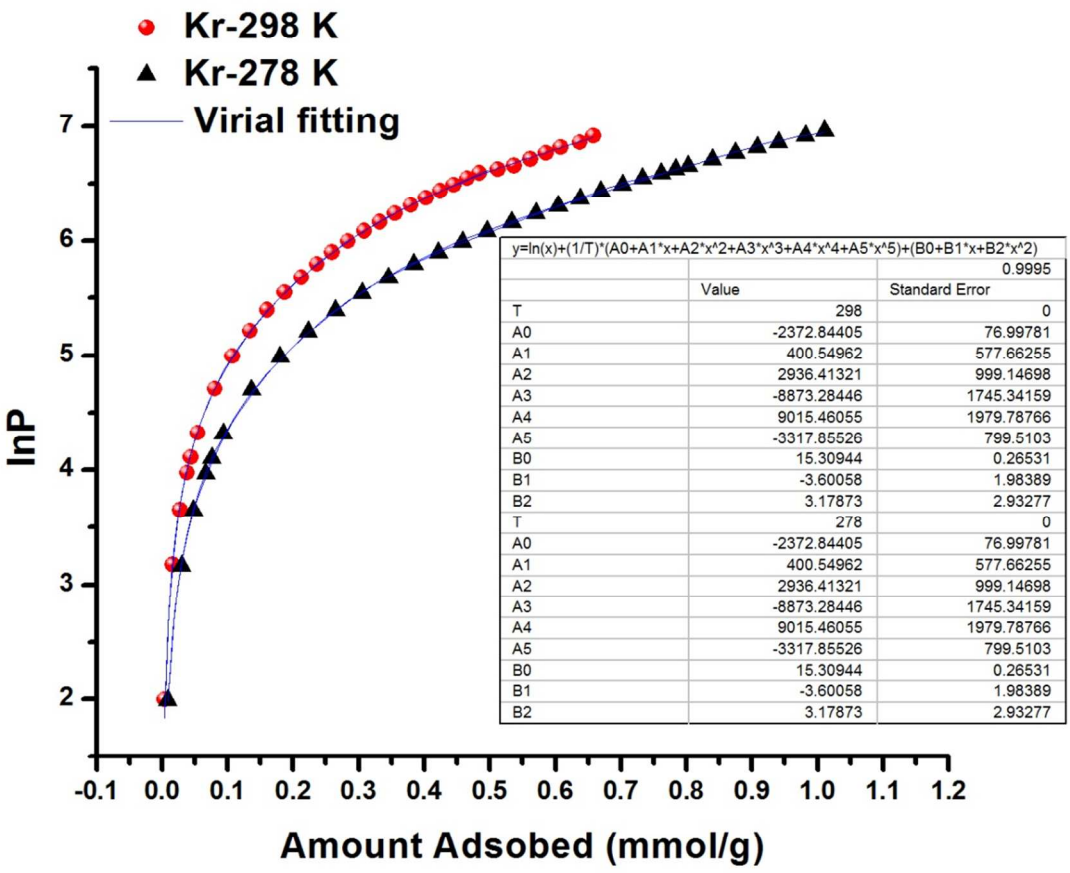

Figure S5. Kr adsorption isotherm of SAPO-34 at 298 K and 278 K fitted using Virial equation.

Column breakthrough experiment for Xe/Kr gas mixture:

Experimental column breakthrough measurements were conducted by packing 0.39 g of SAPO-34 sample in a 6.35-cm long and 0.5-cm diameter column. The sample was activated at a proper temperature. Pressurization of the column-containing MOM was accomplished by syringe pump (Teledyne ISCO) directly connected to the system. An inline pressure transducer was used to verify column pressure. The column was cooled to room temperature and the pure He gas was initially flowed to a Stanford Research Residual Gas Analyzer (RGA) for first three minutes, after which the flow of He is stopped and flow of the Xe/Kr gas mixture is introduced to the fixed bed column containing SAPO-34 sample with flow rate of 1 ml/min and total pressure of 1.4 bar at room temperature. Effluent gases were thereby tracked with the RGA, while the gases

breaking through the column were indicated by an increase in the pressure. This ran for the next 12 hours. The experimental set-up of the column breakthrough experiment is presented in Scheme S2.

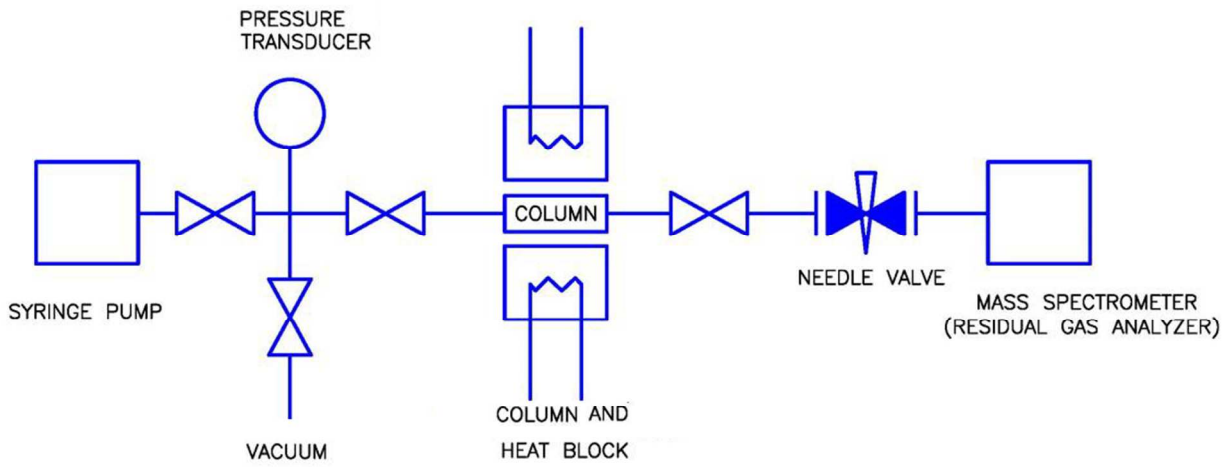

Scheme S1: Schematic representation of the column breakthrough experiment set-up combined with the mass spectrophotometer.

Ideal Adsorbed Solution Theory

The ideal adsorbed solution theory (IAST) was used to predict the selectivity for the binary mixture adsorption of Xe and Kr gases from the experimental pure-gas isotherms. The single-component isotherms were fit to a Langmuir-Freundlich equation (see Figures S5 and S6):

$$q=q_m\times[b\times p/(1+b\times p)]$$

Here, p is the pressure of the bulk gas at equilibrium with the adsorbed phase (kPa), q is the adsorbed amount per mass of adsorbent (mol/kg), q_m is the saturation capacity of adsorption (mol/kg), b is the affinity coefficient (1/kPa).

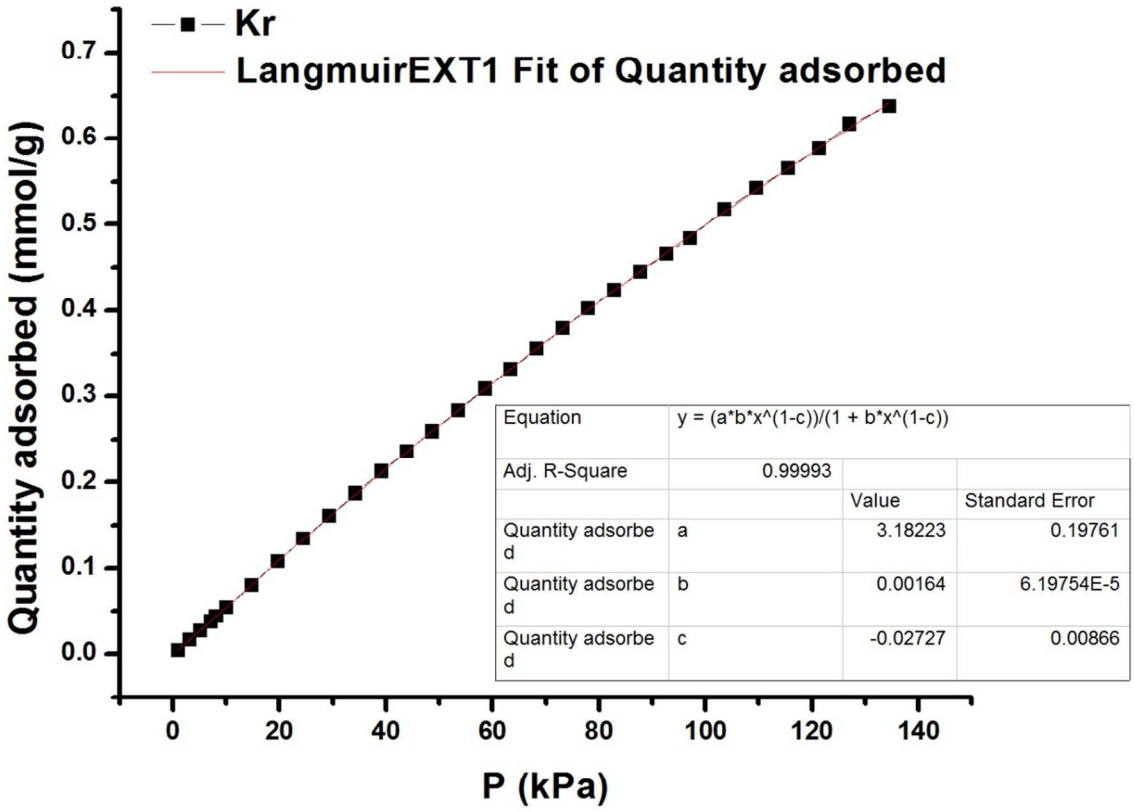

Figure S6. Kr adsorption isotherm of SAPO-34 at 298 K fitted using Langmuir-Freundlich equation.

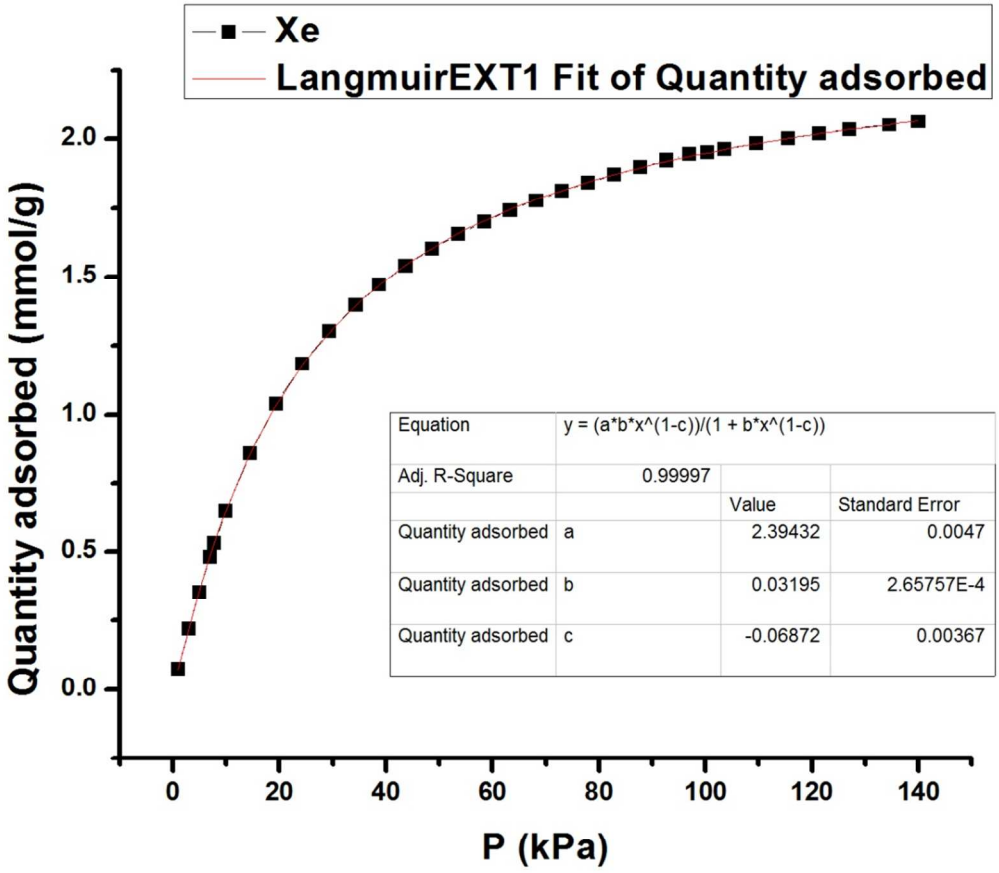

Figure S7. Xe adsorption isotherm of SAPO-34 at 298 K fitted using Langmuir-Freundlich equation.

Modelling membrane permeation and transient breakthroughs in packed beds

The IAST calculations (cf. Figure 2c) show that the adsorption selectivity is in favor of Xe. However, the membrane permeation experiments show that the permeation selectivity is in favor of Kr, i.e. the molecule with the smaller size. The transient experimental breakthrough (cf. Figure 2d) shows that Xe is the component that elutes last, indicating that Xe is preferentially adsorbed. In order to gain further insights into the membrane permeation experiments and transient breakthrough experiments we resorted to modelling. The objectives of our modelling exercise are twofold. Firstly, we wish to gain insights into the intra-crystalline diffusivities of Xe and Kr. Secondly, we wish to demonstrate the compatibility of the membrane permeation data and transient breakthrough experiments.

Let us first consider modelling of membrane permeation employing the simulation methodologies detailed by Krishna (*Micropor. Mesopor. Mater*. **2014,** 185, 30-50; *Phys. Chem. Chem. Phys.* **2016**, 18, 15482-15495). For simulation purposes, the pure component isotherm fits at 298 K were used. Choosing a membrane thickness of δ = 5 μm, we carried out simulations of transient permeation of 90/10 Xe/Kr mixtures with an upstream total pressure of 140 kPa, and downstream pressure ≈ 0 kPa. Two scenarios were investigated with regard to intra-crystalline diffusivities. Firstly, we take equal diffusivities for both Xe and Kr, $\frac{D_{Xe}}{\delta^2} = 0.02$ s^{-1}, and $\frac{D_{Kr}}{\delta^2} = 0.02$ s^{-1}. The transient permeation fluxes are shown in Figure S8. In this scenario, the membrane is selective to Xe and the separation is driving by mixture *adsorption*; the Kr/Xe selectivity is 0.17 at steady-state. The experimental values of Kr/Xe permeation selectivities lie in the range of 12 - 50. Such selectivities can only be realized if molecular sieving effects are in play.

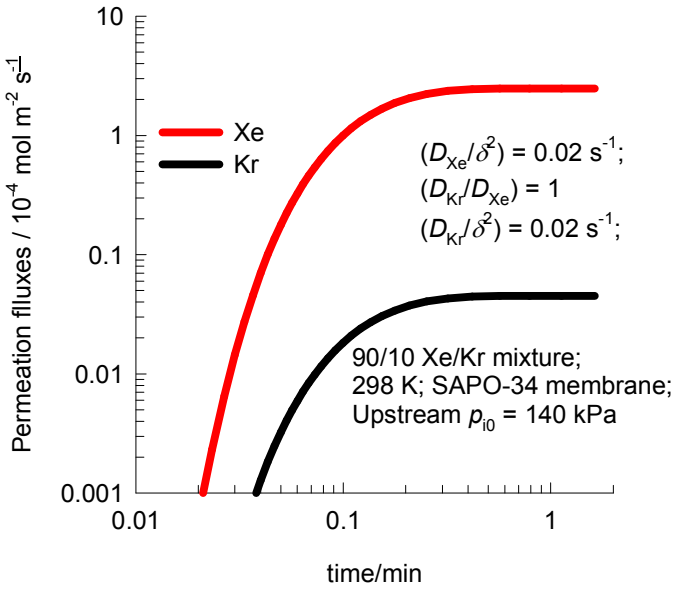

Figure S8. Transient membrane permeation for 90/10 Xe/Kr mixtures assuming equal diffusivities.

In the second scenario, we assume that the diffusivity of Kr is a factor 80 times higher than that of Xe, i.e. $\frac{D_{Xe}}{\delta^2} = 0.02 \ \ s^{-1}$, and $\frac{D_{Kr}}{\delta^2} = 1.6 \ \ s^{-1}$. 80:1 diffusivity ratio was used to get Kr/Xe permeation selectivities > 12 as in the experiments. The permeation fluxes are shown in Figure S9. In this case, the Kr/Xe permeation selectivity at steady-state is 13.1. This leads us to conclude that the experimental data on membrane permeation indicate that the diffusivity of Kr is about two orders of magnitude higher than that of Xe.

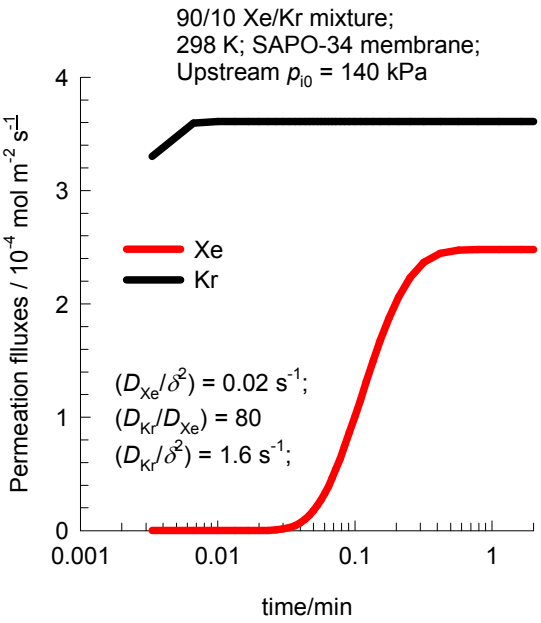

Figure S9. Transient membrane permeation for 90/10 Xe/Kr mixtures assuming that the diffusivity of Kr is 80 times higher than the diffusivity of Xe.

We now model the transient breakthroughs in fixed beds using the simulation methodology as detailed by Krishna (*RSC Adv.* **2015**, *5*, 52269-52295).Two scenarios for the transient breakthrough simulations were employed. In the first scenario, the intra-zeolite diffusion limitations were considered to be negligible. This scenario yields sharp breakthroughs as shown in Figure S10.

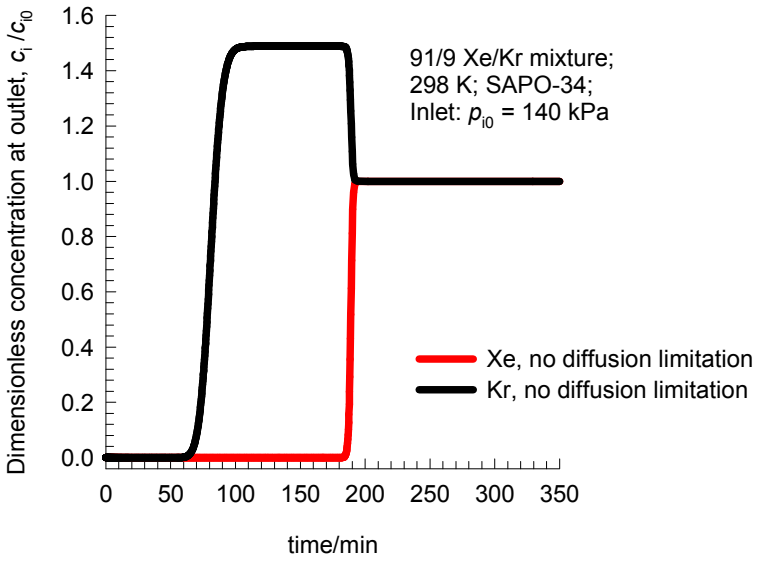

Figure S10. Transient breakthrough simulations for 91/9 Xe/Kr mixtures assuming no intra-crystalline diffusion limitations.

The experimentally observed breakthroughs (cf. Figure 2d) show distended breakthrough characteristics, signifying strong intra-crystalline diffusion limitations. In order to match the experimental breakthroughs, we need to include intra-crystalline diffusivities. For a crystal-radius of r_c, the intra-crystalline diffusion resistances are quantified by two parameters $\frac{D_{Xe}}{r_c^2}$, and $\frac{D_{Kr}}{r_c^2}$. A close match with the experimental breakthroughs (Figure 2d of the main article), are obtained by the choice of diffusivities: $\frac{D_{Xe}}{r_c^2} = 1.25\times10^{-5}$ s^{-1}, and $\frac{D_{Kr}}{r_c^2} = 5\times10^{-5}$ s^{-1}. The diffusivity of Kr is four times higher than that of Xe (Figure S11) .

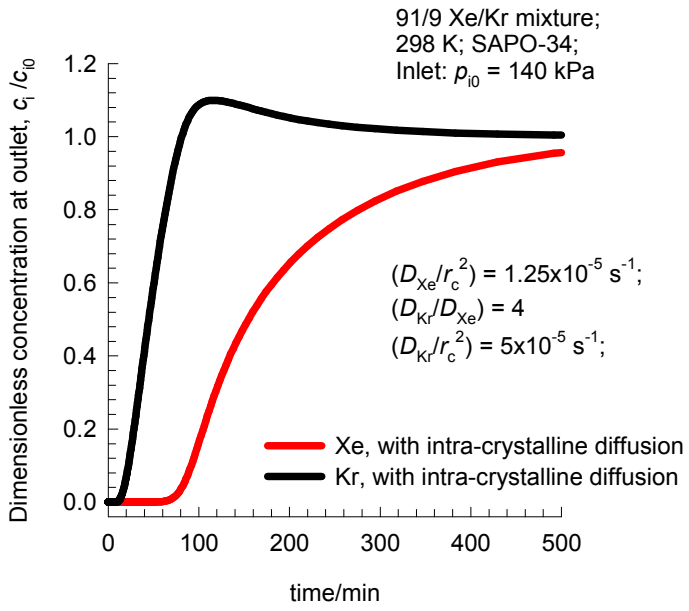

Figure S11. Transient breakthrough simulations for 91/9 Xe/Kr mixtures including intra-crystalline diffusion limitations.

The transient breakthrough simulations lead to two main conclusions: (1) intra-crystalline diffusion resistances cannot be ignored, and (2) the diffusivity of Xe is significantly lower than that of Kr. Both these conclusions are in well agreement with the membrane permeation data.

Table S2. State of the art membranes for *single gas permeation* of Kr and Xe.

Membrane type	Membrane Composition [a]	Kr Permeance (mol/m^2·s·Pa)	Xe Permeance (mol/m^2·s·Pa)	Kr/Xe Ideal Selectivity	Ref.
Polymeric membranes	4-fluoroethylene	3.7×10^{-7}	2.9×10^{-7}	1.3	[1]
	Cellulose acetate	7.3×10^{-12}	2.2×10^{-12}	3.7	[2]
Microporous membranes	Carbon	6.3×10^{-11}	2.1×10^{-11}	3.0	[3]
	DDR	2.9×10^{-10}	5.4×10^{-11}	5.4	
	SAPO-34	2.4×10^{-9}	2.4×10^{-10}	9.9	

[a] Kr selective membranes.

[1] Ohno, M., Ozaki, O., Sato, H., Kimura, S., Miyauchi, T. *J. Nucl. Sci. Technol.* **1977**, 14, 589-602.

[2] Nakai, Y., Yoshimizu, H., Tsujita, Y. *J. Membr. Sci.* **2005**, 256, 72-77.

[3] Zeolite membranes for the separation of krypton and xenon from spent nuclear fuel reprocessing off-gas: Crawford, P. G. M.S. Thesis, Georgia Institute of Technology, Atlanta, GA, 2013.